

Quantized plasmon modes for metallic nanoparticles of arbitrary shape with a generic dielectric function

Marco Romanelli

*Department of Chemical Sciences, University of Padova,
via Marzolo 1, 35131 Padova, Italy*

Gabriel Gil

*Dipartimento di Scienze e Innovazione Tecnologica,
Università degli Studi del Piemonte Orientale Amedeo Avogadro, Alessandria, Italy and
Department of Chemical Sciences, University of Padova,
via Marzolo 1, 35131 Padova, Italy*

Stefano Corni*

*Department of Chemical Sciences, University of Padova,
via Marzolo 1, 35131 Padova, Italy
CNR Institute of Nanoscience, via Campi 213/A, 41125 Modena, Italy and
Padua Quantum Technologies Research Center,
University of Padova, 35131 Padova, Italy*

Abstract

In this work we introduce an effective approach to quantize the electromagnetic response of plasmonic metallic nanostructures. Their shape is arbitrary and they feature a realistic description of the frequency-dependent metal dielectric function that is based on experimental data. The derived quantum modes correctly reproduce the linear response macroscopic polarization of the nanoparticle upon external drive according to classical macroscopic Maxwell equations in the quasistatic limit. Such methodology paves the way for accurate modeling of plexcitonic system, where strong plasmon-molecule coupling and/or strong-driving fields call for a quantized description of the plasmonic response.

Plasmonic metallic nanoparticles (NPs) exhibit coherent and collective oscillations of the metal conduction electrons upon light irradiation. Such phenomenon, referred to as Localized Surface Plasmon Resonance (LSPR), leads to the enhancement of the external electromagnetic field in the proximity of the metal surface, down to molecular scale[1–3]. Over the past decades there has been rising interest in making use of NPs to shape molecular properties by coupling electronic transitions of molecules with the plasmon-enhanced local electromagnetic field arising from LSPRs. This area, known as molecular plasmonics[4], has proved to be an effective non-invasive way of modulating molecular properties as a result of light-matter coupling at the nanoscale. Different applications have been illustrated, showcasing the capability of plasmonic systems to sizably modify molecular photoluminescence[5–9], Raman scattering[10–12], molecular energy transfer[13–16] and excited-state decay[17–19], just to name a few.

Usually, due to the size difference between molecules and metallic NPs, state of the art methods[20–22] tackle these systems by means of multiscale approaches, where the NP response is described by classical electrodynamics while molecules are modeled at ab initio level. Such classical modeling of the NP is expected to break down under strong plasmon-molecule coupling and/or beyond the linear excitation regime, where strong driving fields are considered. Under these regimes, a quantized description of the NP response is unavoidable to capture the correct system dynamics[23, 24].

In the following work, building on a Boundary Element Method (BEM) approach to solve classical macroscopic Maxwell equations in the quasistatic limit, we introduce effective quantum modes to model the optical response of arbitrarily-shaped NPs described by a

generic dielectric function.

Similar approaches based on continuum solutions of the electrodynamics problem were previously introduced[25] and successfully coupled to a quantum chemistry molecular description[26, 27], but in those cases the metal dielectric function is considered to be of simple Drude or Drude-Lorentz (DL) form, thereby constituting a rough approximation to real metal dielectric functions. Indeed, it is well-known that for widely used plasmonic metals, like silver or gold, multiple interband transitions fall in the same spectral region of free-electrons plasmonic resonances, thus making those analytical models inaccurate to properly describe the real dielectric response. To overcome this limitation, the generic dielectric function approach, which relies on fitting a sum of DL oscillators to experimental values of frequency-dependent metal dielectric functions, was recently introduced in a BEM framework[28], opening up the possibility to investigate the electron dynamics of molecules in realistic plasmonic environments. To date, the application of this generic dielectric function approach has been restricted to deal with the classical BEM problem, with its quantized extension is the subject of the present work.

While macroscopic quantum electrodynamics (QED) provides a way to quantize the electromagnetic field (EM) in such environments by introducing a continuum of harmonic oscillators[29], its practical application is limited to cases where perturbative approximations are valid. Indeed, recent works[30–32] have shown that such complex EM continuum structure can be effectively represented by a set of discrete modes that are lossy and coupled, and stem from a system-specific fitting procedure based on the spectral density of the photonic/plasmonic environment of interest. We hereby show that such few-modes effective quantization of the EM continuum via discrete, coupled and lossy modes naturally arise in a quasistatic BEM approach in a way that depends on the dielectric response of the bulk metal, with the effect of the NP shape accounted for numerically but without the need for a fitting procedure. This leads to the identification of the linear response matrix of a quantum system from which quantization of the NP response is achieved. This result shows that the possibility of writing the response of a NP in terms of a set of discrete, coupled and lossy modes is a general feature of nanostructures, at least in the quasi-static response framework.

Theory—In the quasistatic BEM approach that we consider, also termed Polarizable Continuum Model - Nanoparticle (PCM-NP)[20], the linear response polarization of a given NP due to an external electric field is expressed in terms of a surface charge density lying

on the NP surface. The problem of finding such surface charge density for a given driving field is solved numerically using a BEM strategy based on a tessellation (discretization) of the NP surface. The BEM response equation reads,

$$\mathbf{q}(\omega) = \mathbf{Q}(\omega) \mathbf{V}(\omega) \quad (1)$$

where $\mathbf{q}(\omega)$, $\mathbf{V}(\omega)$ are vectors collecting the polarization charges and the electrostatic potential associated to the external electric field acting at each surface element, respectively. On the other hand, $\mathbf{Q}(\omega)$ is the PCM-NP response matrix defined as

$$\mathbf{Q}(\omega) = -\mathbf{S}^{-1} \left(2\pi \frac{\epsilon(\omega) + 1}{\epsilon(\omega) - 1} + \mathbf{DA} \right)^{-1} (2\pi \mathbb{I} + \mathbf{DA}) \quad (2)$$

where \mathbf{S} and \mathbf{D} are the Calderon matrices with elements[33]

$$\begin{aligned} S_{ij} &= \frac{1}{|\vec{s}_i - \vec{s}_j|}, \\ S_{ii} &= 1.0694 \sqrt{A_i/4\pi}, \\ D_{ij} &= \frac{(\vec{s}_i - \vec{s}_j) \cdot \vec{n}_j}{|\vec{s}_i - \vec{s}_j|^3}, \\ D_{ii} &= -(2\pi + \sum_{k \neq i} D_{ik} A_k) 1/A_i. \end{aligned} \quad (3)$$

The \mathbf{A} matrix stores the area of each surface element (also called "tessera") of the NP discretized surface, whereas $\epsilon(\omega)$ is the frequency-dependent dielectric function defining the optical dielectric response.

Following ref.[28], eqs.1-2 are recast as

$$\mathbf{q}(\omega) = -\frac{1}{2\pi} f(\omega) [\mathbf{AD}^\dagger \mathbf{q}(\omega) + \mathbf{S}^{-1} (2\pi \mathbb{I} + \mathbf{DA}) \mathbf{V}(\omega)] \quad (4)$$

with

$$f(\omega) = \frac{\epsilon(\omega) - 1}{\epsilon(\omega) + 1}. \quad (5)$$

For a specific metal, the experimental $f(\omega)$ data is fitted to a sum of N DL-like poles,

$$f(\omega) = \frac{\epsilon(\omega) - 1}{\epsilon(\omega) + 1} \approx \sum_p^N \frac{A_p}{\omega_p^2 - \omega^2 - i\gamma_p \omega}. \quad (6)$$

By introducing the fitting functional form of $f(\omega)$ into eq.4, the polarization charges can be decomposed as pole-dependent charges, i.e. $\mathbf{q}(\omega) = \sum_p^N \mathbf{q}_p(\omega)$, leading to a matrix equation for each pole-dependent charge vector $\mathbf{q}_p(\omega)$:

$$\frac{2\pi}{A_p} (\omega_p^2 - \omega^2 - i\gamma_p \omega) \mathbf{q}_p(\omega) = -[\mathbf{AD}^\dagger \sum_{p'}^N \mathbf{q}_{p'}(\omega) + \mathbf{S}^{-1} (2\pi \mathbb{I} + \mathbf{DA}) \mathbf{V}(\omega)]. \quad (7)$$

As such, the PCM-NP linear response equation within the generic dielectric function approach consists of a problem of coupled damped and driven classical harmonic oscillators. Our goal is therefore to map eq.7 to the linear charge density response of a quantum NP, so that its linear response polarization matches the macroscopic classical one. As shown previously in the simple DL dielectric function case[27], such quantization approach corresponds to a macroscopic-QED quantization of the electromagnetic fields in the same dielectric environment[25–27].

To this end it is convenient to recast eq.6 as

$$f(\omega) \approx \sum_p^N \frac{A_p}{\omega_p^2 - \omega^2 - i\gamma_p\omega} = \sum_p^N \frac{A_p}{2\bar{\omega}_p} \left(\frac{1}{\bar{\omega}_p - \omega - i\gamma_p/2} + \frac{1}{\bar{\omega}_p + \omega + i\gamma_p/2} \right) \quad (8)$$

where $\bar{\omega}_p = \sqrt{\omega_p^2 - \gamma_p^2/4}$. Eq.8 allows us to explicitly deal with the resonant and anti-resonant terms hidden in eq.6. This is a critical step for obtaining a set of coupled quantum oscillators representing the exact (classical) polarization response of the macroscopic system. Indeed, on the basis of eq. 8, the response charges can be decomposed as $\mathbf{q}(\omega) = \sum_p^N \mathbf{q}_p^R(\omega) + \mathbf{q}_p^A(\omega)$, where $\mathbf{q}_p^R(\omega)$, $\mathbf{q}_p^A(\omega)$ respectively arise from the resonant and anti-resonant terms of eq.8. Similarly to the DL case[27], we now express the PCM-NP kernel in its diagonal form via the eigenmode expansion ($\mathbf{S}^{-1/2} \mathbf{D} \mathbf{A} \mathbf{S}^{1/2} = \mathbf{T} \boldsymbol{\lambda} \mathbf{T}^\dagger$, note that only the geometry of the NP, not the nature of the material is involved in this step). To clarify the meaning of such eigenmodes, it is useful to note that for a sphere they correspond to surface charge distributions with different multipolar characters (dipole, quadrupole, etc.). Upon using such eigenmode expansion and the decomposition of eq.8, eq.7 can be recast as (SI 1),

$$\begin{aligned} & (\mathbf{S}^{1/2} \mathbf{T} \mathbf{K}_{pp}^{R/A}(\omega) \mathbf{T}^\dagger \mathbf{S}^{1/2}) \mathbf{q}_p^{R/A}(\omega) + \sum_{p' \neq p}^N \left(\mathbf{S}^{1/2} \mathbf{T} \tilde{\boldsymbol{\lambda}}_{pp'} \mathbf{T}^\dagger \mathbf{S}^{1/2} \right) \mathbf{q}_{p'}^{R/A}(\omega) + \\ & \sum_{p'}^N \left(\mathbf{S}^{1/2} \mathbf{T} \tilde{\boldsymbol{\lambda}}_{pp'} \mathbf{T}^\dagger \mathbf{S}^{1/2} \right) \mathbf{q}_{p'}^{A/R}(\omega) = -\mathbf{V}(\omega) \end{aligned} \quad (9)$$

where $\mathbf{K}_{pp}^R(\omega)$, $\mathbf{K}_{pp}^A(\omega)$ and $\tilde{\boldsymbol{\lambda}}_{pp'}$ are diagonal matrices on the surface element eigenmode index θ :

$$\begin{aligned} (K_{pp}^R(\omega))_{\theta\theta} &= \frac{\frac{4\pi\bar{\omega}_p}{A_p}(\bar{\omega}_p - \omega - i\frac{\gamma_p}{2}) + \lambda_\theta}{2\pi + \lambda_\theta}, \\ (K_{pp}^A(\omega))_{\theta\theta} &= \frac{\frac{4\pi\bar{\omega}_p}{A_p}(\bar{\omega}_p + \omega + i\frac{\gamma_p}{2}) + \lambda_\theta}{2\pi + \lambda_\theta}, \\ (\tilde{\lambda}_{pp'})_{\theta\theta} &= \frac{\lambda_\theta}{2\pi + \lambda_\theta}. \end{aligned} \quad (10)$$

Further manipulation of eqs.9-10 (see SI 1), leads to independent PCM-NP response equations for each θ th BEM eigenmode, reading

$$\left[\begin{pmatrix} \mathbb{A}_\theta & \mathbb{B}_\theta \\ \mathbb{B}_\theta^* & \mathbb{A}_\theta^* \end{pmatrix} - \omega \begin{pmatrix} \mathbb{I} & 0 \\ 0 & -\mathbb{I} \end{pmatrix} \right] \begin{pmatrix} \mathbb{Q}_\theta^R(\omega) \\ \mathbb{Q}_\theta^A(-\omega) \end{pmatrix} = - \begin{pmatrix} \mathbb{V}_\theta(\omega) \\ \mathbb{V}_\theta^*(-\omega) \end{pmatrix} \quad (11)$$

where $\mathbb{A}_\theta, \mathbb{B}_\theta$ are $N \times N$ matrices, whereas $\mathbb{Q}_\theta^{R/A}, \mathbb{V}_\theta$ are N -dimensional vectors whose elements read

$$\begin{aligned} (\mathbb{A}_\theta)_{pp'} &= \left(\bar{\omega}_p - i \frac{\gamma_p}{2} + \lambda_\theta \frac{A_p}{4\pi\bar{\omega}_p} \right) \delta_{pp'} + (1 - \delta_{pp'}) \sqrt{\frac{A_p}{2\bar{\omega}_p}} \frac{\lambda_\theta}{2\pi} \sqrt{\frac{A_{p'}}{2\bar{\omega}_{p'}}} \\ (\mathbb{B}_\theta)_{pp'} &= \sqrt{\frac{A_p}{2\bar{\omega}_p}} \frac{\lambda_\theta}{2\pi} \left(\sqrt{\frac{A_{p'}}{2\bar{\omega}_{p'}}} \right)^* \\ \mathbb{Q}_{\theta,p}^R(\omega) &= \frac{1}{\sqrt{\frac{A_p}{2\bar{\omega}_p} \left(1 + \frac{\lambda_\theta}{2\pi} \right)}} \sum_k (T^\dagger S^{1/2})_{\theta k} q_{p,k}^R(\omega) \\ \mathbb{Q}_{\theta,p}^A(-\omega) &= \frac{1}{\left(\sqrt{\frac{A_p}{2\bar{\omega}_p} \left(1 + \frac{\lambda_\theta}{2\pi} \right)} \right)^*} \sum_k (T^\dagger S^{1/2})_{\theta k} q_{p,k}^A(\omega) \\ \mathbb{V}_{\theta,p}(\omega) &= \text{sgn}(A_p) \left(\sqrt{\frac{A_p}{2\bar{\omega}_p} \left(1 + \frac{\lambda_\theta}{2\pi} \right)} \right)^* \sum_k (T^\dagger S^{-1/2})_{\theta k} V_k(\omega) \\ \mathbb{V}_{\theta,p}^*(-\omega) &= \text{sgn}(A_p) \sqrt{\frac{A_p}{2\bar{\omega}_p} \left(1 + \frac{\lambda_\theta}{2\pi} \right)} \sum_k (T^\dagger S^{-1/2})_{\theta k} V_k(\omega). \end{aligned} \quad (12)$$

Further details on the matrices $\mathbb{A}_\theta, \mathbb{B}_\theta$ as well as a graphical representation of their structure is given in SI 1.

Notably, the shape of the classical PCM-NP response equations for each θ th BEM eigenmode (eq.11) strongly resembles the shape of the linear response equation of a quantum system (as in time-dependent density functional theory)[34–37],

$$\left[\begin{pmatrix} \mathbb{A} & \mathbb{B} \\ \mathbb{B}^* & \mathbb{A}^* \end{pmatrix} - \omega \begin{pmatrix} \mathbb{I} & 0 \\ 0 & -\mathbb{I} \end{pmatrix} \right] \begin{pmatrix} \mathbb{X}(\omega) \\ \mathbb{Y}(-\omega) \end{pmatrix} = - \begin{pmatrix} \mathbb{V}(\omega) \\ \mathbb{V}^*(-\omega) \end{pmatrix} \quad (13)$$

where the matrix \mathbb{A} usually contains single particle excitation frequencies along the diagonal and couplings among them in the off-diagonal blocks, whereas \mathbb{B} couples excitations and de-excitations. $\mathbb{X}(\omega), \mathbb{Y}(-\omega)$ respectively contain the Fourier transformed resonant and anti-resonant transition amplitudes describing the first-order change in the system density matrix upon perturbation, while $\mathbb{V}(\omega)$ and $\mathbb{V}^*(-\omega)$ store matrix elements of the perturbation.

By comparing eq.11 with eq.13 we can achieve quantization of the classical PCM-NP model with generic dielectric function. This is done by mapping the \mathbb{A}_θ and \mathbb{B}_θ matrices to the \mathbb{A} and \mathbb{B} blocks of the linear response matrix of a quantum system featuring single particle plasmonic excitation frequencies $\bar{\omega}_p + \lambda_\theta \frac{A_p}{4\pi\bar{\omega}_p}$ and damping rates $\gamma_p/2$. In turn, $\mathbb{V}_\theta(\omega)$ can be identified with the external perturbation and therefore $\mathbb{Q}_\theta^R(\omega)$ with $\mathbb{X}(\omega)$ and $\mathbb{Q}_\theta^A(-\omega)$ with $\mathbb{Y}(-\omega)$. In other words, the classical macroscopic polarization equation (eq.1) of the NP can be exactly mapped to the linear response polarization of a quantum system composed of a set of coupled and damped quantum plasmon modes for each θ th geometric BEM eigenmode of the NP, independently.

By following standard response theory[34, 36] (SI 1 for details), for each θ we can solve the generalized eigenvalue problem associated with eq.13:

$$\begin{pmatrix} \mathbb{A}_\theta & \mathbb{B}_\theta \\ \mathbb{B}_\theta^* & \mathbb{A}_\theta^* \end{pmatrix} \mathbf{U}_\theta = \begin{pmatrix} \mathbb{I} & 0 \\ 0 & -\mathbb{I} \end{pmatrix} \mathbf{U}_\theta \mathbf{d}_\theta \quad (14)$$

where \mathbf{d}_θ is the diagonal eigenvalue matrix with elements $d_{\theta,n} = \omega_{\theta,n} - i\frac{\gamma_{\theta,n}}{2}$ and $d_{\theta,-n} = -\omega_{\theta,n} - i\frac{\gamma_{\theta,n}}{2}$ for resonant and anti-resonant transitions, respectively. \mathbf{U}_θ collects in its columns the corresponding generalized eigenvectors. Their properties are recalled in SI 1. From eq.14 we can identify $\omega_{\theta,n}$ with the true excitation energy of the quantum NP plasmonic state $|\theta, n\rangle$ with decay rate $\frac{\gamma_{\theta,n}}{2}$ for each θ BEM eigenmode. This leads to the following NP plasmonic Hamiltonian,

$$\hat{H}_{NP} = \sum_{\theta,n} \left(\omega_{\theta,n} - i\frac{\gamma_{\theta,n}}{2} \right) \hat{b}_{\theta,n}^\dagger \hat{b}_{\theta,n} \quad (15)$$

which can be coupled to any quantum chemistry molecular description as detailed in ref.[38].

Moreover, we can also identify within this picture transition elements of relevant operators. Focusing on surface charges, similarly to ref. [27] upon introducing the quantized surface charge operator for the k -th surface tessera \hat{q}_k , the quantum transition charges for each coupled $|\theta, p\rangle$ state can be identified:

$$\langle 0 | \hat{q}_k | \theta, p \rangle = (S^{-1/2}T)_{k\theta} \sqrt{\frac{A_p}{2\bar{\omega}_p} \left(1 + \frac{\lambda_\theta}{2\pi} \right)} \quad (16)$$

leading in turn to

$$\langle 0 | \hat{q}_k | \theta, n \rangle = \sum_p (S^{-1/2}T)_{k\theta} \left[\sqrt{\frac{A_p}{2\bar{\omega}_p} \left(1 + \frac{\lambda_\theta}{2\pi} \right)} X_{\theta,pn} + \left(\sqrt{\frac{A_p}{2\bar{\omega}_p} \left(1 + \frac{\lambda_\theta}{2\pi} \right)} \right)^* Y_{\theta,pn} \right]. \quad (17)$$

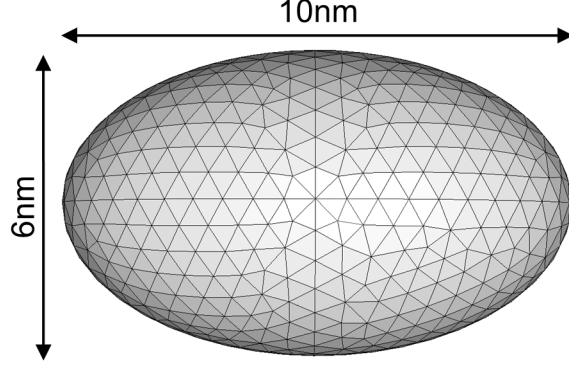


FIG. 1. Ellipsoidal NP model used for simulations featuring 1371 surface tesserae.

Based on eqs.17 and response theory[34, 36] (SI 1 for details), the dipole-dipole polarizability tensor $\alpha_{ab}(\omega)$ of the quantum NP can be expressed in its spectral form as

$$\alpha_{ab}(\omega) = \sum_{\theta,n} \frac{\langle 0 | \hat{\mu}_a | \theta, n \rangle \langle \theta, n | \hat{\mu}_b | 0 \rangle}{\omega_{\theta,n} - \omega - i \frac{\gamma_{\theta,n}}{2}} + \frac{\langle 0 | \hat{\mu}_a | \theta, n \rangle^* \langle \theta, n | \hat{\mu}_b | 0 \rangle^*}{\omega_{\theta,n} + \omega + i \frac{\gamma_{\theta,n}}{2}} \quad (18)$$

where $\hat{\mu}_a$ is defined as $\hat{\mu}_a = \sum_k \hat{q}_k \vec{r}_{k,a}$ with $\vec{r}_{k,a}$ being the a th component of the position vector pointing to the k th NP tessera. Eq.(18) holds for all positive A_p . A slightly more complex expression is obtained in the general case (see SI).

We stress that the plasmonic states so introduced should be regarded as effective states that describe the more complex electronic structure of the true metal NP, featuring quasi-continuum bands, and that they do not constitute exact eigenstates of any unperturbed Hamiltonian. If this were the case, the \mathbb{B}_θ block would be exactly zero according to response theory from exact states[36]. This is clearly not the case for a finite NP, where \mathbb{B}_θ is non-vanishing. Interestingly, for an infinitely planar plasmonic surface λ_θ would be zero[39], making the coupling blocks vanishing.

Numerical results—The theory presented above has been numerically validated on a test case NP of ellipsoidal shape (Fig.1) either made of silver or gold. These two widely used plasmonic metals are well-known to exhibit multiple interband transitions that cannot be captured by a simple DL dielectric function model, thereby making a generic dielectric function approach desirable in these cases. The corresponding function $f(\omega)$ (eq.6) has been fitted to data from ref.[40] for Ag and ref.[41] for Au. The fitted pole parameters are reported in SI 2. In Fig.2 the imaginary part of the NP polarizability, which is proportional to the NP absorption cross-section, is shown for both silver (Fig.2a) and gold (Fig.2b). The

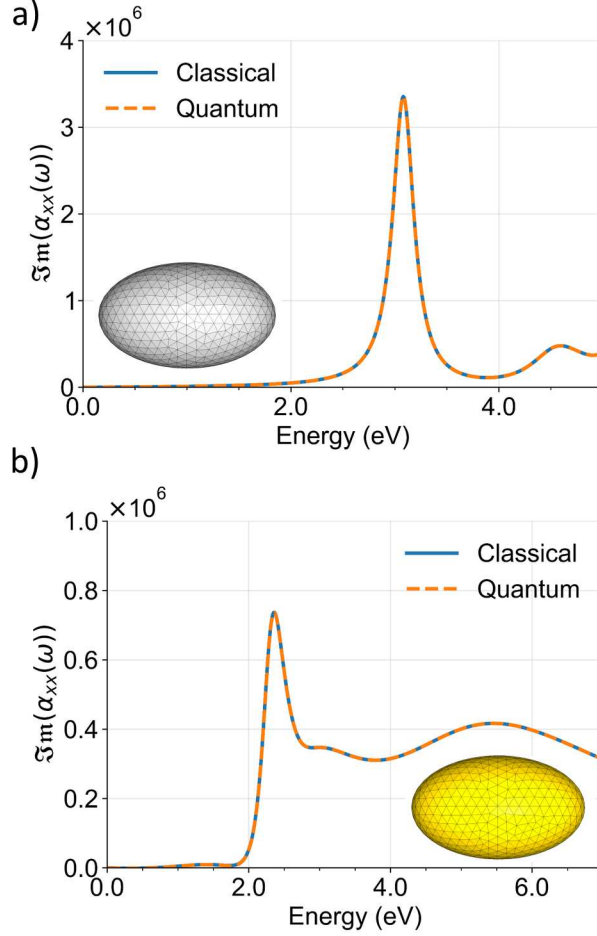


FIG. 2. Imaginary part of the xx component of the dipole-dipole polarizability tensor for the ellipsoidal NP (Fig.1) when the $f(\omega)$ function is fitted to Ag Brendel-Bormann[40] (a) or Au Etchegoin[41] (b) reference data. The classical PCM-NP (solid blue) and quantum Q-PCM-NP (dashed orange) results are shown.

classical result (solid blue) is obtained from the induced dipole moment of the NP upon numerical solution of eq.1, while the quantum result (dashed orange) is computed according to eq.18. Since in the quasi-static limit only the dipolar mode is contributing to the NP optical response only that mode is considered here (SI 2). The driving field is oriented along the main axis of the ellipsoidal NP (x axis) and so the $\alpha_{xx}(\omega)$ component of the polarizability tensor is analyzed. Fig.2 clearly shows that the here introduced quantum states of the NP correctly reproduce the classical macroscopic polarization of the NP in both cases, thus validating the quantization procedure detailed above. The real part of the polarizability is also correctly reproduced, as shown in Figs. S3.

Concluding remarks—In this work, we have laid down an effective quantum modes description to model the optical response of arbitrarily-shaped NPs endowed with empirical dielectric functions. The linear response polarization of the quantum NP correctly recovers the classical result obtained by solving the macroscopic Maxwell equations in the quasistatic limit via BEM. It is worth remarking that although the NP linear response is usually well-described by classical electrodynamics, the quantization of the NP response is of utmost importance when the coupling with an external quantum emitter (i.e. molecule) is investigated. Indeed, the classical model is known to provide faulty behaviors both in the strong-coupling and strong-driving regimes[23, 24], making it inadequate to realistically model plexcitonic systems. Since BEM has extensively proven to be a convenient framework to model ab initio molecules in complex plasmonic environments[20, 26, 42], the development here presented paves the way for a fully quantum description of plexcitonic systems, composed of NPs of arbitrary shape and made of realistic metals.

Acknowledgments—The authors acknowledge Giulia Dall’Osto for insightful preliminary discussions on the generic dielectric function fitting procedure. The authors also acknowledge the C3P HPC facility of the Department of Chemical Sciences of the University of Padua for providing the computational resources supporting this work.

* stefano.corni@unipd.it

- [1] V. Giannini, A. I. Fernández-Domínguez, S. C. Heck, and S. A. Maier, Plasmonic nanoantennas: fundamentals and their use in controlling the radiative properties of nanoemitters, *Chem. Rev.* **111**, 3888 (2011).
- [2] K. M. Mayer and J. H. Hafner, Localized surface plasmon resonance sensors, *Chem. Rev.* **111**, 3828 (2011).
- [3] W. A. Murray and W. L. Barnes, Plasmonic materials, *Adv. Mater.* **19**, 3771 (2007).
- [4] F. Della Sala and S. D’Agostino, *Handbook of molecular plasmonics* (Pan Stanford Publishing, Singapore, 2013).
- [5] J. R. Lakowicz, C. D. Geddes, I. Gryczynski, J. Malicka, Z. Gryczynski, K. Aslan, J. Lukomska, E. Matveeva, J. Zhang, R. Badugu, *et al.*, Advances in surface-enhanced fluorescence, *J. Fluoresc.* **14**, 425 (2004).

- [6] J. R. Lakowicz, Radiative decay engineering 5: metal-enhanced fluorescence and plasmon emission, *Anal. Biochem.* **337**, 171 (2005).
- [7] P. Anger, P. Bharadwaj, and L. Novotny, Enhancement and quenching of single-molecule fluorescence, *Phys. Rev. Lett.* **96**, 113002 (2006).
- [8] B. Yang, G. Chen, A. Ghafoor, Y. Zhang, Y. Zhang, Y. Zhang, Y. Luo, J. Yang, V. Sandoghdar, J. Aizpurua, *et al.*, Sub-nanometre resolution in single-molecule photoluminescence imaging, *Nat. Photonics* **14**, 693 (2020).
- [9] M. Romanelli, G. Dall'Osto, and S. Corni, Role of metal-nanostructure features on tip-enhanced photoluminescence of single molecules, *J. Chem. Phys.* **155**, 214304 (2021).
- [10] J. Lee, K. T. Crampton, N. Tallarida, and V. Apkarian, Visualizing vibrational normal modes of a single molecule with atomically confined light, *Nature* **568**, 78 (2019).
- [11] G. Dall'Osto and S. Corni, Time-dependent surface-enhanced raman scattering: A theoretical approach, *J. Chem. Phys.* **161** (2024).
- [12] X. Wang, S.-C. Huang, S. Hu, S. Yan, and B. Ren, Fundamental understanding and applications of plasmon-enhanced raman spectroscopy, *Nat. Rev. Phys.* **2**, 253 (2020).
- [13] S. Cao, A. Rosławska, B. Doppagne, M. Romeo, M. Féron, F. Chérioux, H. Bulou, F. Scheurer, and G. Schull, Energy funnelling within multichromophore architectures monitored with sub-nanometre resolution, *Nat. Chem.* **13**, 766 (2021).
- [14] H. Imada, K. Miwa, M. Imai-Imada, S. Kawahara, K. Kimura, and Y. Kim, Single-molecule investigation of energy dynamics in a coupled plasmon-exciton system, *Phys. Rev. Lett.* **119**, 013901 (2017).
- [15] F.-F. Kong, X.-J. Tian, Y. Zhang, Y. Zhang, G. Chen, Y.-J. Yu, S.-H. Jing, H.-Y. Gao, Y. Luo, J.-L. Yang, *et al.*, Wavelike electronic energy transfer in donor-acceptor molecular systems through quantum coherence, *Nat. Nanotechnol.* **17**, 729 (2022).
- [16] C. V. Coane, M. Romanelli, G. Dall'Osto, R. Di Felice, and S. Corni, Unraveling the mechanism of tip-enhanced molecular energy transfer, *Commun. Chem.* **7**, 32 (2024).
- [17] S. Felicetti, J. Fregoni, T. Schnappinger, S. Reiter, R. de Vivie-Riedle, and J. Feist, Photo-protecting uracil by coupling with lossy nanocavities, *J. Phys. Chem. Lett.* **11**, 8810 (2020).
- [18] J. Torres-Sánchez and J. Feist, Molecular photodissociation enabled by ultrafast plasmon decay, *J. Chem. Phys.* **154**, 014303 (2021).
- [19] J. Kutttruff, M. Romanelli, E. Pedrueza-Villalmanzo, J. Allerbeck, J. Fregoni, V. Saavedra-

- Becerril, J. Andréasson, D. Brida, A. Dmitriev, S. Corni, *et al.*, Sub-picosecond collapse of molecular polaritons to pure molecular transition in plasmonic photoswitch-nanoantennas, *Nat. Commun.* **14**, 3875 (2023).
- [20] B. Mennucci and S. Corni, Multiscale modelling of photoinduced processes in composite systems, *Nature Reviews Chemistry* **3**, 315 (2019).
- [21] J. Fregoni, F. J. Garcia-Vidal, and J. Feist, Theoretical challenges in polaritonic chemistry, *ACS Photonics* **9**, 1096 (2022).
- [22] M. Capone, M. Romanelli, D. Castaldo, G. Parolin, A. Bello, G. Gil, and M. Vanzan, A vision for the future of multiscale modeling, *ACS Phys. Chem. Au.* **4**, 202 (2024).
- [23] E. Waks and D. Sridharan, Cavity qed treatment of interactions between a metal nanoparticle and a dipole emitter, *Phys. Rev. A* **82**, 043845 (2010).
- [24] M. Romanelli and S. Corni, Identifying differences between semiclassical and full-quantum descriptions of plexcitons, *J. Phys. Chem. Lett.* **15**, 9326 (2024).
- [25] A. Trügler and U. Hohenester, Strong coupling between a metallic nanoparticle and a single molecule, *Phys. Rev. B Condens. Matter* **77**, 115403 (2008).
- [26] T. Neuman, R. Esteban, D. Casanova, F. J. García-Vidal, and J. Aizpurua, Coupling of molecular emitters and plasmonic cavities beyond the point-dipole approximation, *Nano Lett.* **18**, 2358 (2018).
- [27] J. Fregoni, T. S. Haugland, S. Pipolo, T. Giovannini, H. Koch, and S. Corni, Strong coupling between localized surface plasmons and molecules by coupled cluster theory, *Nano Lett.* **21**, 6664 (2021).
- [28] G. Dall’Osto, G. Gil, S. Pipolo, and S. Corni, Real-time dynamics of plasmonic resonances in nanoparticles described by a boundary element method with generic dielectric function, *J. Chem. Phys.* **153** (2020).
- [29] B. Huttner and S. M. Barnett, Quantization of the electromagnetic field in dielectrics, *Phys. Rev. A* **46**, 4306 (1992).
- [30] I. Medina, F. J. García-Vidal, A. I. Fernández-Domínguez, and J. Feist, Few-mode field quantization of arbitrary electromagnetic spectral densities, *Phys. Rev. Lett.* **126**, 093601 (2021).
- [31] M. Sánchez-Barquilla, F. J. García-Vidal, A. I. Fernández-Domínguez, and J. Feist, Few-mode field quantization for multiple emitters, *Nanophotonics* **11**, 4363 (2022).
- [32] C. J. S. Martínez, J. Feist, and F. J. García-Vidal, A mixed perturbative-nonperturbative

- treatment for strong light-matter interactions, *Nanophotonics* **13**, 2669 (2024).
- [33] J. Tomasi, B. Mennucci, and R. Cammi, Quantum mechanical continuum solvation models, *Chem. Rev.* **105**, 2999 (2005).
 - [34] R. McWeeny, *Methods of Molecular Quantum Mechanics*, 2nd ed. (Academic Press, San Diego, California, U.S., 1992).
 - [35] S. Corni and J. Tomasi, Excitation energies of a molecule close to a metal surface, *The Journal of Chemical Physics* **117**, 7266 (2002).
 - [36] P. Norman, K. Ruud, and T. Saue, *Principles and practices of molecular properties: Theory, modeling, and simulations* (Wiley, Hoboken, New Jersey, U.S., 2018).
 - [37] H. Ye, J. C. Becca, and L. Jensen, Modeling the near-field effect on molecular excited states using the discrete interaction model/quantum mechanical method, *J. Chem. Phys.* **160** (2024).
 - [38] J. Fregoni, G. Granucci, M. Persico, and S. Corni, Strong coupling with light enhances the photoisomerization quantum yield of azobenzene, *Chem* **6**, 250 (2020).
 - [39] S. Corni, S. Pipolo, and R. Cammi, Equation of motion for the solvent polarization apparent charges in the polarizable continuum model: Application to real-time tddft, *The Journal of Physical Chemistry A* **119**, 5405 (2015).
 - [40] A. D. Rakić, A. B. Djurišić, J. M. Elazar, and M. L. Majewski, Optical properties of metallic films for vertical-cavity optoelectronic devices, *Appl. Opt.* **37**, 5271 (1998).
 - [41] P. G. Etchegoin, E. Le Ru, and M. Meyer, An analytic model for the optical properties of gold, *J. Chem. Phys.* **125** (2006).
 - [42] M. Romanelli, R. R. Riso, T. S. Haugland, E. Ronca, S. Corni, and H. Koch, Effective single-mode methodology for strongly coupled multimode molecular-plasmon nanosystems, *Nano Lett.* **23**, 4938 (2023).

Supplementary material for:

**Quantized plasmon modes for metallic
nanoparticles of arbitrary shape with a generic
dielectric function**

Marco Romanelli,[†] Gabriel Gil,^{‡,†} and Stefano Corni^{*,†,¶,§}

[†]*Department of Chemical Sciences, University of Padova, via Marzolo 1, 35131 Padova,
Italy*

[‡]*Dipartimento di Scienze e Innovazione Tecnologica, Università degli Studi del Piemonte
Orientale Amedeo Avogadro, Alessandria, Italy.*

[¶]*CNR Institute of Nanoscience, via Campi 213/A, 41125 Modena, Italy*

[§]*Padua Quantum Technologies Research Center, University of Padova, 35131 Padova, Italy*

E-mail: stefano.corni@unipd.it

Contents

1	Q-PCM-NP with generic dielectric function	3
2	Computational details	12
3	Real part of $\alpha_{xx}(\omega)$ for the ellipsoidal NP of Figs.1-2	15
	References	16

1 Q-PCM-NP with generic dielectric function

The goal of this section is to manipulate the classical PCM-NP equation so to arrive to a format that is identical to the response equation of a quantum system.

Within the generic dielectric function approach,¹ the classical PCM-NP equations read

$$\mathbf{q}(\omega) = \frac{1}{2\pi} f(\omega) \mathbf{F}(\omega) \quad (\text{S1})$$

with

$$\mathbf{F}(\omega) = -[\mathbf{A}\mathbf{D}^\dagger \mathbf{q}(\omega) + \mathbf{S}^{-1} (2\pi\mathbb{I} + \mathbf{D}\mathbf{A}) \mathbf{V}(\omega)] \quad (\text{S2})$$

and

$$f(\omega) = \frac{\epsilon(\omega) - 1}{\epsilon(\omega) + 1} \approx \sum_p^N \frac{A_p}{\omega_p^2 - \omega^2 - i\gamma_p\omega}. \quad (\text{S3})$$

As discussed in ref.,¹ using eq.S3 the classical response charges of eq.S1 can be decomposed as pole-dependent charges as $\mathbf{q}(\omega) = \sum_p^N \mathbf{q}_p(\omega)$, turning eq.S1 into

$$\frac{2\pi}{A_p} (\omega_p^2 - \omega^2 - i\gamma_p\omega) \mathbf{q}_p(\omega) = -[\mathbf{A}\mathbf{D}^\dagger \mathbf{q}(\omega) + \mathbf{S}^{-1} (2\pi\mathbb{I} + \mathbf{D}\mathbf{A}) \mathbf{V}(\omega)]. \quad (\text{S4})$$

To achieve quantization (Q-PCM-NP) it is more convenient to explicitly express the resonant and anti-resonant contributions hidden in eq.S3 as

$$f(\omega) \approx \sum_p^N \frac{A_p}{\omega_p^2 - \omega^2 - i\gamma_p\omega} = \sum_p^N \frac{A_p}{2\bar{\omega}_p} \left(\frac{1}{\bar{\omega}_p - \omega - i\gamma_p/2} + \frac{1}{\bar{\omega}_p + \omega + i\gamma_p/2} \right) \quad (\text{S5})$$

with

$$\bar{\omega}_p = \sqrt{\omega_p^2 - \gamma_p^2/4}. \quad (\text{S6})$$

The first term in round brackets of eq.S5 can be defined as the resonant term (R, $\propto (\bar{\omega}_p - \omega)^{-1}$) while the other one is the anti-resonant (A, $\propto (\bar{\omega}_p + \omega)^{-1}$). Consequently, the classical response charges can be further decomposed as $\mathbf{q}(\omega) = \sum_p^N \mathbf{q}_p(\omega) = \sum_p^N \mathbf{q}_p^R(\omega) + \mathbf{q}_p^A(\omega)$,

which turns eq.S4 into two separate coupled equations for each pth pole,

$$\begin{aligned}\frac{4\pi\bar{\omega}_p}{A_p}(\bar{\omega}_p - \omega - i\frac{\gamma_p}{2})\mathbf{q}_p^R(\omega) &= -[\mathbf{A}\mathbf{D}^\dagger \sum_{p'}^N (\mathbf{q}_{p'}^R(\omega) + \mathbf{q}_{p'}^A(\omega)) + \mathbf{S}^{-1}(2\pi\mathbb{I} + \mathbf{D}\mathbf{A})\mathbf{V}(\omega)] , \\ \frac{4\pi\bar{\omega}_p}{A_p}(\bar{\omega}_p + \omega + i\frac{\gamma_p}{2})\mathbf{q}_p^A(\omega) &= -[\mathbf{A}\mathbf{D}^\dagger \sum_{p'}^N (\mathbf{q}_{p'}^R(\omega) + \mathbf{q}_{p'}^A(\omega)) + \mathbf{S}^{-1}(2\pi\mathbb{I} + \mathbf{D}\mathbf{A})\mathbf{V}(\omega)] .\end{aligned}\tag{S7}$$

Furthermore, by turning the BEM kernel in diagonal form as shown in refs^{2,3} via the eigenmode decomposition ($\mathbf{S}^{-1/2}\mathbf{D}\mathbf{A}\mathbf{S}^{1/2} = \mathbf{T}\boldsymbol{\lambda}\mathbf{T}^\dagger$) and by left-multiplying each eq.S7 by \mathbf{S} (while considering the following relations³ $\mathbf{S} = \mathbf{S}^{\frac{1}{2}}\mathbf{S}^{\frac{1}{2}}$, $\mathbf{S}\mathbf{A}\mathbf{D}^\dagger = \mathbf{D}\mathbf{A}\mathbf{S}$), straightforward matrix algebra leads to

$$\begin{aligned}(\mathbf{S}^{1/2}\mathbf{T}\mathbf{K}_{pp}^R(\omega)\mathbf{T}^\dagger\mathbf{S}^{1/2})\mathbf{q}_p^R(\omega) + \sum_{p' \neq p}^N \left(\mathbf{S}^{1/2}\mathbf{T}\tilde{\boldsymbol{\lambda}}_{pp'}\mathbf{T}^\dagger\mathbf{S}^{1/2} \right) \mathbf{q}_{p'}^R(\omega) + \\ \sum_{p'}^N \left(\mathbf{S}^{1/2}\mathbf{T}\tilde{\boldsymbol{\lambda}}_{pp'}\mathbf{T}^\dagger\mathbf{S}^{1/2} \right) \mathbf{q}_{p'}^A(\omega) = -\mathbf{V}(\omega) , \\ (\mathbf{S}^{1/2}\mathbf{T}\mathbf{K}_{pp}^A(\omega)\mathbf{T}^\dagger\mathbf{S}^{1/2})\mathbf{q}_p^A(\omega) + \sum_{p' \neq p}^N \left(\mathbf{S}^{1/2}\mathbf{T}\tilde{\boldsymbol{\lambda}}_{pp'}\mathbf{T}^\dagger\mathbf{S}^{1/2} \right) \mathbf{q}_{p'}^A(\omega) + \\ \sum_{p'}^N \left(\mathbf{S}^{1/2}\mathbf{T}\tilde{\boldsymbol{\lambda}}_{pp'}\mathbf{T}^\dagger\mathbf{S}^{1/2} \right) \mathbf{q}_{p'}^R(\omega) = -\mathbf{V}(\omega)\end{aligned}\tag{S8}$$

with

$$\begin{aligned}K_{pp,\theta\theta}^R(\omega) &= \frac{\frac{4\pi\bar{\omega}_p}{A_p}(\bar{\omega}_p - \omega - i\frac{\gamma_p}{2}) + \lambda_\theta}{2\pi + \lambda_\theta} = \frac{\bar{\omega}_p - \omega - i\frac{\gamma_p}{2} + \lambda_\theta \frac{A_p}{4\pi\bar{\omega}_p}}{\frac{A_p}{2\bar{\omega}_p} \left(1 + \frac{\lambda_\theta}{2\pi} \right)} , \\ K_{pp,\theta\theta}^A(\omega) &= \frac{\frac{4\pi\bar{\omega}_p}{A_p}(\bar{\omega}_p + \omega + i\frac{\gamma_p}{2}) + \lambda_\theta}{2\pi + \lambda_\theta} = \frac{\bar{\omega}_p + \omega + i\frac{\gamma_p}{2} + \lambda_\theta \frac{A_p}{4\pi\bar{\omega}_p}}{\frac{A_p}{2\bar{\omega}_p} \left(1 + \frac{\lambda_\theta}{2\pi} \right)} , \\ \tilde{\lambda}_{pp',\theta\theta} &= \frac{\lambda_\theta}{2\pi + \lambda_\theta} .\end{aligned}\tag{S9}$$

Note that the matrices of eq.S9 are diagonal in $\theta\theta'$ and the absence of pp' indexes on the right-hand side of $\tilde{\lambda}_{pp',\theta\theta} = \frac{\lambda_\theta}{2\pi + \lambda_\theta}$ means that these coupling matrix elements do not depend

on the pole indexes, but only on the BEM eigenmode one (θ). Note that since the matrix $\mathbf{S}^{-1/2} \mathbf{D} \mathbf{A} \mathbf{S}^{1/2}$ is real and symmetric, the λ_θ eigenvalues are also all real.

Making explicit matrix multiplication, eq.S8 reads

$$\begin{aligned}
& \sum_{\theta k} (S^{1/2} T)_{j\theta} K_{pp,\theta\theta}^R (T^\dagger S^{1/2})_{\theta k} q_{pk}^R + \sum_{\theta k} \sum_{p' \neq p}^N (S^{1/2} T)_{j\theta} \tilde{\lambda}_{pp',\theta\theta} (T^\dagger S^{1/2})_{\theta k} q_{p'k}^R + \\
& \sum_{\theta k} \sum_{p'}^N (S^{1/2} T)_{j\theta} \tilde{\lambda}_{pp',\theta\theta} (T^\dagger S^{1/2})_{\theta k} q_{p'k}^A = -V_j, \\
& \sum_{\theta k} (S^{1/2} T)_{j\theta} K_{pp,\theta\theta}^A (T^\dagger S^{1/2})_{\theta k} q_{pk}^A + \sum_{\theta k} \sum_{p' \neq p}^N (S^{1/2} T)_{j\theta} \tilde{\lambda}_{pp',\theta\theta} (T^\dagger S^{1/2})_{\theta k} q_{p'k}^A + \\
& \sum_{\theta k} \sum_{p'}^N (S^{1/2} T)_{j\theta} \tilde{\lambda}_{pp',\theta\theta} (T^\dagger S^{1/2})_{\theta k} q_{p'k}^R = -V_j
\end{aligned} \tag{S10}$$

where the (ω) have been dropped to ease notation and $q_{pk}^{R/A} = q_{pk}^{R/A}(\omega)$ represents the k th surface classical resonant/anti-resonant response charge due to the p th pole. $V_j = V_j(\omega)$ is instead the external potential acting on the j th surface tessera.

Upon defining $\tilde{q}_{\theta p}^R = \sum_k (T^\dagger S^{1/2})_{\theta k} q_{pk}^R$, $\tilde{q}_{\theta p}^A = \sum_k (T^\dagger S^{1/2})_{\theta k} q_{pk}^A$ and $\tilde{V}_{\theta p} = \sum_j (T^\dagger S^{-1/2})_{\theta j} V_j$ eq.S10 can be recast as

$$\begin{aligned}
& K_{pp,\theta\theta}^R \tilde{q}_{\theta p}^R + \sum_{p' \neq p}^N \tilde{\lambda}_{pp',\theta\theta} \tilde{q}_{\theta p'}^R + \sum_{p'}^N \tilde{\lambda}_{pp',\theta\theta} \tilde{q}_{\theta p'}^A = -\tilde{V}_{\theta p}, \\
& K_{pp,\theta\theta}^A \tilde{q}_{\theta p}^A + \sum_{p' \neq p}^N \tilde{\lambda}_{pp',\theta\theta} \tilde{q}_{\theta p'}^A + \sum_{p'}^N \tilde{\lambda}_{pp',\theta\theta} \tilde{q}_{\theta p'}^R = -\tilde{V}_{\theta p}.
\end{aligned} \tag{S11}$$

Note that we have added a p subscript to the potential \tilde{V} to make the terms of the equations uniform, but that $\tilde{V}_{\theta p}$ is actually independent from p .

Further manipulation of eq.S11 finally leads to

$$\begin{aligned}
& \left(\bar{\omega}_p - i\frac{\gamma_p}{2} + \lambda_\theta \frac{A_p}{4\pi\bar{\omega}_p} \right) \mathbb{Q}_{\theta p}^R - \omega \mathbb{Q}_{\theta p}^R + \sum_{p' \neq p}^N \sqrt{\frac{A_p}{2\bar{\omega}_p} \left(1 + \frac{\lambda_\theta}{2\pi} \right)} \tilde{\lambda}_{pp',\theta\theta} \sqrt{\frac{A_{p'}}{2\bar{\omega}_{p'}} \left(1 + \frac{\lambda_\theta}{2\pi} \right)} \mathbb{Q}_{\theta p'}^R + \\
& \sum_{p'}^N \sqrt{\frac{A_p}{2\bar{\omega}_p} \left(1 + \frac{\lambda_\theta}{2\pi} \right)} \tilde{\lambda}_{pp',\theta\theta} \left(\sqrt{\frac{A_{p'}}{2\bar{\omega}_{p'}} \left(1 + \frac{\lambda_\theta}{2\pi} \right)} \right)^* \mathbb{Q}_{\theta p'}^A = -\mathbb{V}_{\theta p}, \\
& \left(\bar{\omega}_p + i\frac{\gamma_p}{2} + \lambda_\theta \frac{A_p}{4\pi\bar{\omega}_p} \right) \mathbb{Q}_{\theta p}^A + \omega \mathbb{Q}_{\theta p}^A + \sum_{p' \neq p}^N \left(\sqrt{\frac{A_p}{2\bar{\omega}_p} \left(1 + \frac{\lambda_\theta}{2\pi} \right)} \right)^* \tilde{\lambda}_{pp',\theta\theta} \left(\sqrt{\frac{A_{p'}}{2\bar{\omega}_{p'}} \left(1 + \frac{\lambda_\theta}{2\pi} \right)} \right)^* \\
& \mathbb{Q}_{\theta p'}^A + \sum_{p'}^N \left(\sqrt{\frac{A_p}{2\bar{\omega}_p} \left(1 + \frac{\lambda_\theta}{2\pi} \right)} \right)^* \tilde{\lambda}_{pp',\theta\theta} \left(\sqrt{\frac{A_{p'}}{2\bar{\omega}_{p'}} \left(1 + \frac{\lambda_\theta}{2\pi} \right)} \right) \mathbb{Q}_{\theta p'}^R = -\mathbb{V}_{\theta p}^*,
\end{aligned} \tag{S12}$$

where

$$\begin{aligned}
\mathbb{Q}_{\theta p}^R &= \frac{1}{\sqrt{\frac{A_p}{2\bar{\omega}_p} \left(1 + \frac{\lambda_\theta}{2\pi} \right)}} \tilde{q}_{\theta p}^R \\
\mathbb{Q}_{\theta p}^A &= \frac{1}{\left(\sqrt{\frac{A_p}{2\bar{\omega}_p} \left(1 + \frac{\lambda_\theta}{2\pi} \right)} \right)^*} \tilde{q}_{\theta p}^A \\
\mathbb{V}_{\theta p} &= \text{sgn}(A_p) \left(\sqrt{\frac{A_p}{2\bar{\omega}_p} \left(1 + \frac{\lambda_\theta}{2\pi} \right)} \right)^* \tilde{V}_{\theta p} \\
\mathbb{V}_{\theta p}^* &= \text{sgn}(A_p) \sqrt{\frac{A_p}{2\bar{\omega}_p} \left(1 + \frac{\lambda_\theta}{2\pi} \right)} \tilde{V}_{\theta p}.
\end{aligned} \tag{S13}$$

The $\text{sgn}(A_p)$ in the last two equations is needed to take into account that some A_p may be negative, as described and explained in ref.¹ In practice, we are translating this into a modified perturbation whose matrix elements have a change of sign for those $|\theta, p\rangle$ that corresponds to negative A_p .

Recalling the form of $\tilde{\lambda}_{pp',\theta\theta}$ (eq.S9) eq.S12 can be further simplified to

$$\begin{aligned}
& \left(\bar{\omega}_p - i\frac{\gamma_p}{2} + \lambda_\theta \frac{A_p}{4\pi\bar{\omega}_p} \right) \mathfrak{q}_{\theta p}^R - \omega \mathfrak{q}_{\theta p}^R + \sum_{p' \neq p}^N \sqrt{\frac{A_p}{2\bar{\omega}_p}} \frac{\lambda_\theta}{2\pi} \sqrt{\frac{A_{p'}}{2\bar{\omega}_{p'}}} \mathfrak{q}_{\theta p'}^R + \\
& \sum_{p'}^N \sqrt{\frac{A_p}{2\bar{\omega}_p}} \frac{\lambda_\theta}{2\pi} \left(\sqrt{\frac{A_{p'}}{2\bar{\omega}_{p'}}} \right)^* \mathfrak{q}_{\theta p'}^A = -\mathbb{V}_{\theta p}, \\
& \left(\bar{\omega}_p + i\frac{\gamma_p}{2} + \lambda_\theta \frac{A_p}{4\pi\bar{\omega}_p} \right) \mathfrak{q}_{\theta p}^A + \omega \mathfrak{q}_{\theta p}^A + \sum_{p' \neq p}^N \left(\sqrt{\frac{A_p}{2\bar{\omega}_p}} \right)^* \frac{\lambda_\theta}{2\pi} \left(\sqrt{\frac{A_{p'}}{2\bar{\omega}_{p'}}} \right)^* \mathfrak{q}_{\theta p'}^A + \\
& \sum_{p'}^N \left(\sqrt{\frac{A_p}{2\bar{\omega}_p}} \right)^* \frac{\lambda_\theta}{2\pi} \left(\sqrt{\frac{A_{p'}}{2\bar{\omega}_{p'}}} \right) \mathfrak{q}_{\theta p'}^R = -\mathbb{V}_{\theta p}^*.
\end{aligned} \tag{S14}$$

Basically, for each θ th BEM eigenmode eq.S14 corresponds to an independent matrix equation of the following form

$$\left[\begin{pmatrix} \mathbb{A}_\theta & \mathbb{B}_\theta \\ \mathbb{B}_\theta^* & \mathbb{A}_\theta^* \end{pmatrix} - \omega \begin{pmatrix} \mathbb{I} & 0 \\ 0 & -\mathbb{I} \end{pmatrix} \right] \begin{pmatrix} \mathfrak{q}_\theta^R \\ \mathfrak{q}_\theta^A \end{pmatrix} = - \begin{pmatrix} \mathbb{V}_\theta \\ \mathbb{V}_\theta^* \end{pmatrix} \tag{S15}$$

with

$$\begin{aligned}
(\mathbb{A}_\theta)_{pp'} &= \left(\bar{\omega}_p - i\frac{\gamma_p}{2} + \lambda_\theta \frac{A_p}{4\pi\bar{\omega}_p} \right) \delta_{pp'} + (1 - \delta_{pp'}) \sqrt{\frac{A_p}{2\bar{\omega}_p}} \frac{\lambda_\theta}{2\pi} \sqrt{\frac{A_{p'}}{2\bar{\omega}_{p'}}} \\
(\mathbb{B}_\theta)_{pp'} &= \sqrt{\frac{A_p}{2\bar{\omega}_p}} \frac{\lambda_\theta}{2\pi} \left(\sqrt{\frac{A_{p'}}{2\bar{\omega}_{p'}}} \right)^*
\end{aligned} \tag{S16}$$

and $\mathfrak{q}_\theta^{R/A}, \mathbb{V}_\theta$ are vectors of dimension N (n. of poles in eq.S3) which store the corresponding p th elements $\mathfrak{q}_{\theta,p}^{R/A}, \mathbb{V}_{\theta,p}$.

To give a graphical illustration of the matrices $\mathbb{A}_\theta, \mathbb{B}_\theta$, in the hypothetical case of 3 poles ($N=3$), the matrices would look

$$\begin{aligned}
\mathbb{A}_\theta &= \begin{pmatrix} \overline{\overline{K}}_{11,\theta\theta} & \overline{\overline{\lambda}}_{12,\theta\theta} & \overline{\overline{\lambda}}_{13,\theta\theta} \\ \overline{\overline{\lambda}}_{12,\theta\theta} & \overline{\overline{K}}_{22,\theta\theta} & \overline{\overline{\lambda}}_{23,\theta\theta} \\ \overline{\overline{\lambda}}_{13,\theta\theta} & \overline{\overline{\lambda}}_{23,\theta\theta} & \overline{\overline{K}}_{33,\theta\theta} \end{pmatrix} \\
\mathbb{B}_\theta &= \begin{pmatrix} \overline{\overline{\eta}}_{11,\theta\theta} & \overline{\overline{\eta}}_{12,\theta\theta} & \overline{\overline{\eta}}_{13,\theta\theta} \\ \overline{\overline{\eta}}_{12,\theta\theta}^* & \overline{\overline{\eta}}_{22,\theta\theta} & \overline{\overline{\eta}}_{23,\theta\theta} \\ \overline{\overline{\eta}}_{13,\theta\theta}^* & \overline{\overline{\eta}}_{23,\theta\theta}^* & \overline{\overline{\eta}}_{33,\theta\theta} \end{pmatrix}
\end{aligned} \tag{S17}$$

with $\overline{\overline{K}}_{pp,\theta\theta} = \left(\overline{\omega}_p - i\frac{\gamma_p}{2} + \lambda_\theta \frac{A_p}{4\pi\overline{\omega}_p} \right)$, $\overline{\overline{\lambda}}_{pp',\theta\theta} = \sqrt{\frac{A_p}{2\overline{\omega}_p}} \frac{\lambda_\theta}{2\pi} \sqrt{\frac{A_{p'}}{2\overline{\omega}_{p'}}}$ and $\overline{\overline{\eta}}_{pp',\theta\theta} = \sqrt{\frac{A_p}{2\overline{\omega}_p}} \frac{\lambda_\theta}{2\pi} \left(\sqrt{\frac{A_{p'}}{2\overline{\omega}_{p'}}} \right)^*$. Note that \mathbb{A}_θ is not hermitian because of the imaginary damping rates, whereas \mathbb{B}_θ is.

Notably, the form of eq.S15 bears a strong similarity with the matrix structure of the linear response equation of a quantum system. Indeed, standard linear response theory⁴⁻⁶ leads to the following general matrix equation

$$\left[\begin{pmatrix} \mathbb{A} & \mathbb{B} \\ \mathbb{B}^* & \mathbb{A}^* \end{pmatrix} - \omega \begin{pmatrix} \mathbb{I} & 0 \\ 0 & -\mathbb{I} \end{pmatrix} \right] \begin{pmatrix} \mathbb{X} \\ \mathbb{Y} \end{pmatrix} = - \begin{pmatrix} \mathbb{V} \\ \mathbb{V}^* \end{pmatrix} \tag{S18}$$

where the matrices \mathbb{A}, \mathbb{B} store single particle excitations of the system and couplings among them, whereas \mathbb{X}, \mathbb{Y} respectively contains the Fourier transformed resonant and anti-resonant transition amplitudes describing the first-order change in the system density matrix upon perturbation. \mathbb{V} and \mathbb{V}^* respectively store matrix elements of the perturbation.

By comparing eq.S15 and eq.S18, it can be observed that the classical PCM-NP equations in the generic dielectric function approach can be exactly mapped to the linear response

equations of a quantum system for each θ th BEM eigenmode independently, where

$$\begin{aligned}
\mathbb{A} &= \mathbb{A}_\theta \\
\mathbb{B} &= \mathbb{B}_\theta \\
\mathbb{X} &= \mathbb{Q}_\theta^R \\
\mathbb{Y} &= \mathbb{Q}_\theta^A \\
\mathbb{V} &= \mathbb{V}_\theta .
\end{aligned} \tag{S19}$$

Following this mapping, we can identify the diagonal element $(\mathbb{A}_\theta)_{pp}$ with the p th single particle transition frequency of the quantum NP due to the θ th BEM eigenmode $(\bar{\omega}_p + \lambda_\theta \frac{A_p}{4\pi\bar{\omega}_p})$ and corresponding damping rate $(\frac{\gamma_p}{2})$, while $\bar{\lambda}_{pp',\theta\theta}$ constitute coupling matrix elements between such transitions. Furthermore, upon introducing the quantized surface charge operator \hat{q} as in refs.,^{2,7} we identify the quantum transition charge sitting on the k th tessera as

$$\langle 0 | \hat{q}_k | \theta, p \rangle = (S^{-1/2}T)_{k\theta} \sqrt{\frac{A_p}{2\bar{\omega}_p} \left(1 + \frac{\lambda_\theta}{2\pi} \right)} \tag{S20}$$

for each $|\theta, p\rangle$ quantum plasmon mode originating from each p th pole of the generic dielectric function for a given θ th BEM eigenmode. Note that simulations reported in main text were performed restricting θ to the dipolar mode only θ_{dip} , as it is the only relevant mode contributing to the NP optical response in the quasi-static limit. Inclusion of additional modes of higher order is straightforward since each θ th eigenmode leads to an independent response equation which does not couple to the response of other modes (eq.S15). The same approximation has been coherently applied to the classical PCM-NP equations by setting to zero the contribution to the classical response charges from higher-order modes.

To complete the discussion on the mapping between classical and quantum modes, it is useful to consider the perturbation element $\mathbb{V}_{\theta p}$ and how it can be recast following its

definition eq.S13 and the expression of $\langle 0 | \hat{q}_k | \theta, p \rangle$:

$$\mathbb{V}_{\theta,p} = \sum_j \text{sgn}(A_p) \left(\sqrt{\frac{A_p}{2\omega_p} \left(1 + \frac{\lambda_\theta}{2\pi} \right)} \right)^* (T^\dagger S^{-1/2})_{\theta j} V_j = \sum_j \text{sgn}(A_p) \langle \theta, p | \hat{q}_j | 0 \rangle V_j \quad (\text{S21})$$

which is the expected form of the perturbation over the tesserae (j index), once the change of sign for negative A_p is accounted for.

On the basis of standard response theory,^{4,6} the response matrix can be conveniently recast in its spectral representation. The generalized eigenvalue problem also discussed in the main text

$$\begin{pmatrix} \mathbb{A}_\theta & \mathbb{B}_\theta \\ \mathbb{B}_\theta^* & \mathbb{A}_\theta^* \end{pmatrix} \mathbf{U}_\theta = \begin{pmatrix} \mathbb{I} & 0 \\ 0 & -\mathbb{I} \end{pmatrix} \mathbf{U}_\theta \mathbf{d}_\theta \quad (\text{S22})$$

specifically reads

$$\left[\begin{pmatrix} \mathbb{A}_\theta & \mathbb{B}_\theta \\ \mathbb{B}_\theta^* & \mathbb{A}_\theta^* \end{pmatrix} - (\omega_{\theta,n} - i\frac{\gamma_{\theta,n}}{2}) \begin{pmatrix} \mathbb{I} & 0 \\ 0 & -\mathbb{I} \end{pmatrix} \right] \mathbf{U}_{\theta,n} = 0 \quad (\text{S23})$$

Because of the structure of the response matrix, the eigenvalues come in pairs⁶ (if $\omega_{\theta,n} - i\frac{\gamma_{\theta,n}}{2}$ is an eigenvalue, so it is $-\omega_{\theta,n} - i\frac{\gamma_{\theta,n}}{2}$). Thus it is convenient to use an index n running from 1 to N and from -1 to $-N$ to label them and the eigenvectors: $d_{\theta,n} = \omega_{\theta,n} - i\frac{\gamma_{\theta,n}}{2}$ and $d_{\theta,-n} = -\omega_{\theta,n} - i\frac{\gamma_{\theta,n}}{2}$. The n -th eigenvector, i.e. the n -th column of the matrix \mathbf{U}_θ , $\mathbf{U}_{\theta,n}$, has the structure

$$\mathbf{U}_{\theta,n} = \begin{pmatrix} \mathbf{X}_{\theta,n} \\ \mathbf{Y}_{\theta,n} \end{pmatrix} \quad \mathbf{U}_{\theta,-n} = \begin{pmatrix} \mathbf{Y}_{\theta,n}^* \\ \mathbf{X}_{\theta,n}^* \end{pmatrix} \quad (\text{S24})$$

which leads to

$$\begin{aligned}
\langle 0 | \hat{q}_k | \theta, n \rangle &= \sum_p (\langle 0 | \hat{q}_k | \theta, p \rangle X_{\theta, pn} + \langle \theta, p | \hat{q}_k | 0 \rangle Y_{\theta, pn}) = \\
&= \sum_p (S^{-1/2} T)_{k\theta} \left[\sqrt{\frac{A_p}{2\omega_p} \left(1 + \frac{\lambda_\theta}{2\pi} \right)} X_{\theta, pn} + \left(\sqrt{\frac{A_p}{2\omega_p} \left(1 + \frac{\lambda_\theta}{2\pi} \right)} \right)^* Y_{\theta, pn} \right].
\end{aligned} \tag{S25}$$

Since eq.S22 is a generalized eigenvalue problem, its numerical solution is practically obtained by recasting it into a normal eigenvalue problem where the response matrix features a sign change in the lower row

$$\mathbf{U}_\theta^{-1} \begin{pmatrix} \mathbb{I} & 0 \\ 0 & -\mathbb{I} \end{pmatrix} \begin{pmatrix} \mathbb{A}_\theta & \mathbb{B}_\theta \\ \mathbb{B}_\theta^* & \mathbb{A}_\theta^* \end{pmatrix} \mathbf{U}_\theta = \mathbf{U}_\theta^{-1} \begin{pmatrix} \mathbb{A}_\theta & \mathbb{B}_\theta \\ -\mathbb{B}_\theta^* & -\mathbb{A}_\theta^* \end{pmatrix} \mathbf{U}_\theta = \mathbf{d}_\theta \tag{S26}$$

which is the actual matrix diagonalization performed in practice. By solving eq.S15 for $\mathfrak{q}_\theta^R = \mathbb{X}_\theta$ and $\mathfrak{q}_\theta^A = \mathbb{Y}_\theta$, while making use of eq.S26 it follows,

$$\begin{pmatrix} \mathbb{X}_\theta \\ \mathbb{Y}_\theta \end{pmatrix} = \mathbf{U}_\theta \left[\mathbf{d}_\theta - \omega \begin{pmatrix} \mathbb{I} & 0 \\ 0 & \mathbb{I} \end{pmatrix} \right]^{-1} \mathbf{U}_\theta^{-1} \begin{pmatrix} \mathbb{I} & 0 \\ 0 & -\mathbb{I} \end{pmatrix} \begin{pmatrix} \mathbb{V}_\theta \\ \mathbb{V}_\theta^* \end{pmatrix} \tag{S27}$$

Note that due to the non-hermicity of \mathbb{A}_θ , $\mathbf{U}_\theta^{-1} \neq \mathbf{U}_\theta^\dagger$ and so its n -th row reads

$$\mathbf{U}_{\theta, n}^{-1} = \begin{pmatrix} \mathbf{Z}_{\theta, n} & \mathbf{W}_{\theta, n} \end{pmatrix} \quad \mathbf{U}_{\theta, -n}^{-1} = \begin{pmatrix} \mathbf{W}_{\theta, n}^* & \mathbf{Z}_{\theta, n}^* \end{pmatrix} \tag{S28}$$

allowing the following identification:

$$\begin{aligned}
\langle \theta, n | \hat{q}_k | 0 \rangle &= \sum_p (\langle \theta, p | \hat{q}_k | 0 \rangle Z_{\theta, np} - \langle 0 | \hat{q}_k | \theta, p \rangle W_{\theta, np}) = \\
&= \sum_p (T^\dagger S^{-1/2})_{\theta k} \left[\left(\sqrt{\frac{A_p}{2\bar{\omega}_p}} \left(1 + \frac{\lambda_\theta}{2\pi} \right) \right)^* Z_{\theta, np} - \sqrt{\frac{A_p}{2\bar{\omega}_p}} \left(1 + \frac{\lambda_\theta}{2\pi} \right) W_{\theta, np} \right].
\end{aligned} \tag{S29}$$

Note that in this most general case, rigorously speaking $\langle 0 | \hat{q}_k | \theta, n \rangle^* \neq \langle \theta, n | \hat{q}_k | 0 \rangle$ (although in practice it holds $\langle 0 | \hat{q}_k | \theta, n \rangle^* \approx \langle \theta, n | \hat{q}_k | 0 \rangle$); thus the notation should be understood to refer only approximately to a set of excited states $|\theta, n\rangle$.

On the basis of eqs.S22-S29 and response theory,⁶ the spectral representation of the dipole-dipole polarizability of the quantum NP becomes

$$\begin{aligned}
\alpha_{ab}(\omega) &= \sum_{\theta, n} \frac{\langle 0 | \hat{\mu}_a | \theta, n \rangle \sum_p \text{sgn}(A_p) (\langle \theta, p | \hat{\mu}_b | 0 \rangle Z_{\theta, np} - \langle 0 | \hat{\mu}_b | \theta, p \rangle W_{\theta, np})}{\omega_{\theta, n} - \omega - i \frac{\gamma_{\theta, n}}{2}} + \\
&\quad \frac{\langle 0 | \hat{\mu}_a | \theta, n \rangle^* \left(\sum_p \text{sgn}(A_p) (\langle \theta, p | \hat{\mu}_b | 0 \rangle Z_{\theta, np} - \langle 0 | \hat{\mu}_b | \theta, p \rangle W_{\theta, np}) \right)^*}{\omega_{\theta, n} + \omega + i \frac{\gamma_{\theta, n}}{2}}
\end{aligned} \tag{S30}$$

When there are no negative A_p , this equation can be further simplify to:

$$\alpha_{ab}(\omega) = \sum_{\theta, n} \frac{\langle 0 | \hat{\mu}_a | \theta, n \rangle \langle \theta, n | \hat{\mu}_b | 0 \rangle}{\omega_{\theta, n} - \omega - i \frac{\gamma_{\theta, n}}{2}} + \frac{\langle 0 | \hat{\mu}_a | \theta, n \rangle^* \langle \theta, n | \hat{\mu}_b | 0 \rangle^*}{\omega_{\theta, n} + \omega + i \frac{\gamma_{\theta, n}}{2}} \tag{S31}$$

where $\hat{\mu}_a = \hat{q}_k \vec{r}_{k,a}$ with $\vec{r}_{k,a}$ being the a th component of the position vector pointing to the k th surface NP tessera.

2 Computational details

Simulations reported in main text have been performed on a test case NP of ellipsoidal shape, whose main axis is 10 nm long and the short axis is 6 nm long (Fig. 1). The surface

mesh has been created with the Gmsh⁸ code and features 1371 surface tesserae. The Ag Brendel-Bormann⁹ and Au Etchegoin¹⁰ frequency-dependent data of the metal dielectric functions were fitted as a sum of 4 and 6 DL poles,¹ respectively. The fitting $f(\omega)$ functions are shown in Figs. S1-S2 and the corresponding fitting parameters are given in Tables S1-S2. As mentioned in SI 1 only the dipolar mode $\theta = \theta_{dip}$ has been considered throughout the work since it is the only relevant one for the optical response in the quasi-static limit.

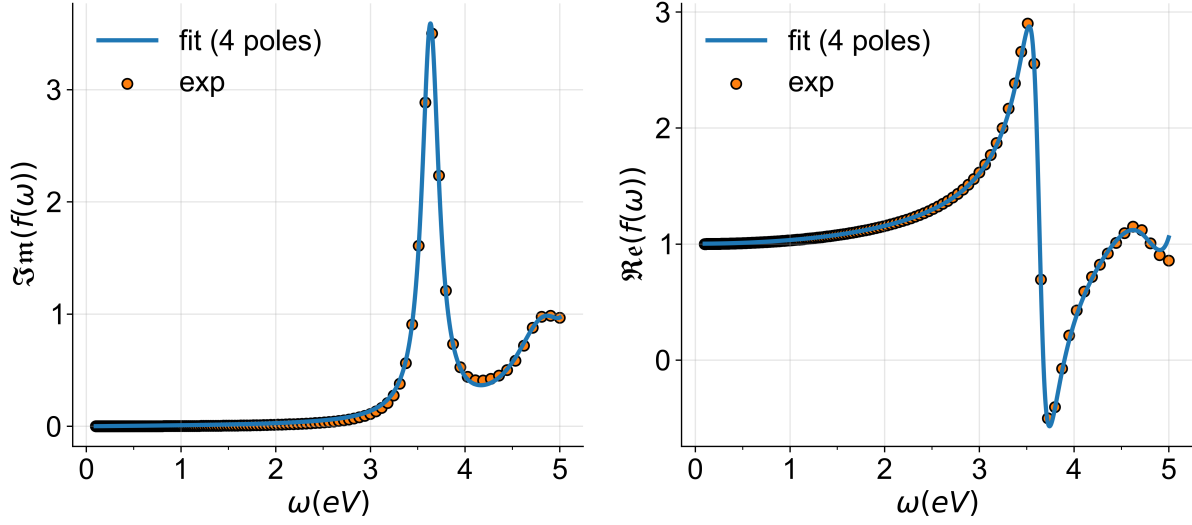


Figure S1: Fitting of Ag $f(\omega)$ function with 4 poles to Brendel-Bormann⁹ reference data (orange dots). The fitting result is the solid blue line. Left and right panels respectively show imaginary and real parts of $f(\omega)$. The fitting parameters are given in Table S1.

Table S1: Fitting pole parameters of $f(\omega)$ for Ag Brendel-Bormann⁹ reference data.

pole n.	ω_p (eV)	γ_p (eV)	A_p (eV ²)
1	3.64	0.219	2.79
2	4.85	0.763	3.33
3	5.18	0.0861	1.51
4	9.89	0.0	58.1

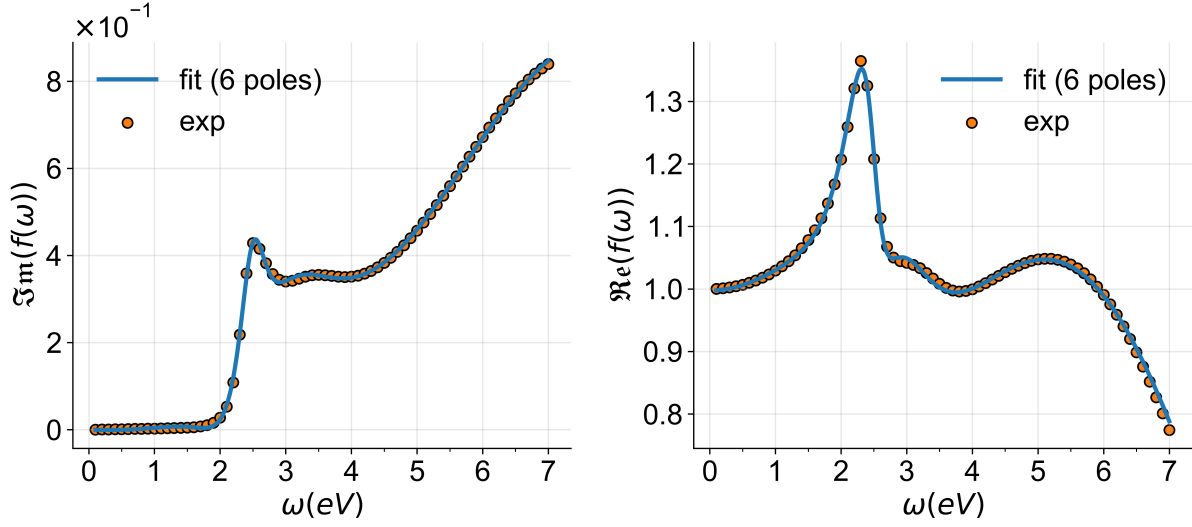


Figure S2: Fitting of Au $f(\omega)$ function with 6 poles to Etchegoin¹⁰ reference data (orange dots). The fitting result is the solid blue line. Left and right panels respectively show imaginary and real parts of $f(\omega)$. The fitting parameters are given in Table S2

Table S2: Fitting pole parameters of $f(\omega)$ for Au Etchegoin¹⁰ reference data.

pole n.	ω_p (eV)	γ_p (eV)	A_p (eV ²)
1	2.51	0.573	0.674
2	2.59	1.76	-5.19
3	2.85	2.34	7.90
4	5.24	9.06	15.4
5	8.39	7.52	63.1
6	42.4	0	643

3 Real part of $\alpha_{xx}(\omega)$ for the ellipsoidal NP of Figs.1-2

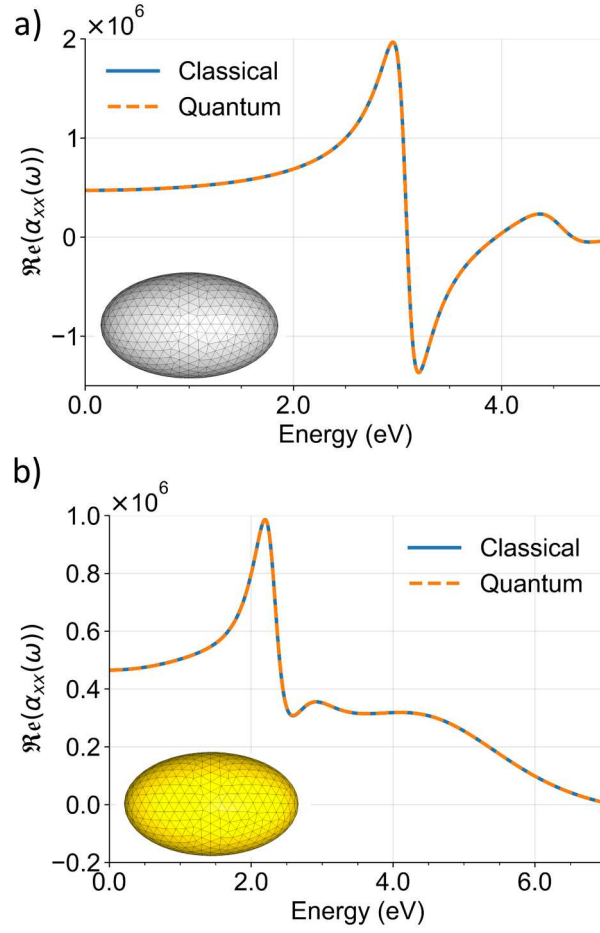


Figure S3: Real part of the xx component of the dipole-dipole polarizability tensor for the ellipsoidal NP (Fig. 1) when the $f(\omega)$ function is fitted to Ag Brendel-Bormann⁹ (a) or Au Etchegoin¹⁰ (b) reference data. The classical PCM-NP (solid blue) and quantum Q-PCM-NP results (dashed orange) are shown.

References

- (1) Dall’Osto, G.; Gil, G.; Pipolo, S.; Corni, S. Real-time dynamics of plasmonic resonances in nanoparticles described by a boundary element method with generic dielectric function. *J. Chem. Phys.* **2020**, *153*.
- (2) Fregoni, J.; Granucci, G.; Persico, M.; Corni, S. Strong coupling with light enhances the photoisomerization quantum yield of azobenzene. *Chem* **2020**, *6*, 250–265.
- (3) Corni, S.; Pipolo, S.; Cammi, R. Equation of motion for the solvent polarization apparent charges in the polarizable continuum model: Application to real-time TDDFT. *The Journal of Physical Chemistry A* **2015**, *119*, 5405–5416.
- (4) Norman, P.; Ruud, K.; Saue, T. *Principles and practices of molecular properties: Theory, modeling, and simulations*; Wiley, Hoboken, New Jersey, U.S., 2018.
- (5) Ye, H.; Becca, J. C.; Jensen, L. Modeling the near-field effect on molecular excited states using the discrete interaction model/quantum mechanical method. *J. Chem. Phys.* **2024**, *160*.
- (6) McWeeny, R. *Methods of Molecular Quantum Mechanics*, 2nd ed.; Academic Press, San Diego, California, U.S., 1992.
- (7) Guido, C. A.; Rosa, M.; Cammi, R.; Corni, S. An open quantum system theory for polarizable continuum models. *J. Chem. Phys.* **2020**, *152*.
- (8) Geuzaine, C.; Remacle, J.-F. Gmsh: A 3-D finite element mesh generator with built-in pre-and post-processing facilities. *International journal for numerical methods in engineering* **2009**, *79*, 1309–1331.
- (9) Rakić, A. D.; Djurišić, A. B.; Elazar, J. M.; Majewski, M. L. Optical properties of metallic films for vertical-cavity optoelectronic devices. *Appl. Opt.* **1998**, *37*, 5271–5283.

- (10) Etchegoin, P. G.; Le Ru, E.; Meyer, M. An analytic model for the optical properties of gold. *J. Chem. Phys.* **2006**, *125*.